ARMY RESEARCH LABORATORY

Modeling of the 105-mm Rarefaction Wave Gun

by Terence P. Coffee

ARL-TR-4897 **August 2009**

NOTICES

Disclaimers

The findings in this report are not to be construed as an official Department of the Army position unless so designated by other authorized documents.

Citation of manufacturer's or trade names does not constitute an official endorsement or approval of the use thereof.

Destroy this report when it is no longer needed. Do not return it to the originator.

Army Research Laboratory
Aberdeen Proving Ground, MD 21005-5066

ARL-TR-4897 **August 2009**

Modeling of the 105-mm Rarefaction Wave Gun

Terence P. Coffee
Weapons and Materials Research Directorate, ARL

REPORT DOCUMENTATION PAGE	Form Approved OMB No. 0704-0188

1. REPORT DATE *(DD-MM-YYYY)*	2. REPORT TYPE	3. DATES COVERED (From - To)
August 2009	Final	May 2006–July 2007

4. TITLE AND SUBTITLE
Modeling of the 105-mm Rarefaction Wave Gun

5a. CONTRACT NUMBER

5b. GRANT NUMBER

5c. PROGRAM ELEMENT NUMBER

6. AUTHOR(S)
Terence P. Coffee

5d. PROJECT NUMBER
622618.H8099

5e. TASK NUMBER

5f. WORK UNIT NUMBER

7. PERFORMING ORGANIZATION NAME(S) AND ADDRESS(ES)
U.S. Army Research Laboratory
ATTN: RDRL-WMB-D
Aberdeen Proving Ground, MD 21005-5066

8. PERFORMING ORGANIZATION REPORT NUMBER
ARL-TR-4897

9. SPONSORING/MONITORING AGENCY NAME(S) AND ADDRESS(ES)

10. SPONSOR/MONITOR'S ACRONYM(S)

11. SPONSOR/MONITOR'S REPORT NUMBER(S)

12. DISTRIBUTION/AVAILABILITY STATEMENT
Approved for public release; distribution is unlimited.

13. SUPPLEMENTARY NOTES

14. ABSTRACT

The Rarefaction wAVE guN (RAVEN) is designed to reduce the recoil momentum of a gun while having a minimal effect on the projectile velocity. The recoil reduction is achieved by venting gas out the breech through an expansion nozzle. This is similar to a recoilless rifle. The difference is that the venting is delayed until the projectile is some distance down tube. The opening of the breech creates a rarefaction wave that travels down the bore of the gun. If the timing is done correctly, the rarefaction wave will not reach the projectile until at or after muzzle exit. Hence, the projectile does not know the breech has opened, and the venting has no effect on the muzzle velocity.

As a proof of principle, a 35-mm RAVEN gun was designed, built, and fired. The breech is a moving piston. When the piston moves a specified distance, it opens a vent into an expanding nozzle. There is a small reduction in the muzzle velocity due to the motion of the breech, i.e., the chamber becomes larger than for a fixed breech gun. If the timing is correct, there is no additional reduction in the muzzle velocity from venting.

In a previous report, a one-dimensional model of the RAVEN was presented. The model covered the interior ballistics, motion of the projectile and the breech, opening of the vent, flow through the nozzle, and blow down of the gun. The model was validated against the 35-mm RAVEN data.

In this report, an updated version of the model is discussed. The modified model is compared with the old 35-mm RAVEN data. The model is then applied to a proposed 105-mm demonstrator. The demonstrator has not yet been built.

15. SUBJECT TERMS
rarefaction wave gun, interior ballistics, recoil

16. SECURITY CLASSIFICATION OF:			17. LIMITATION OF ABSTRACT	18. NUMBER OF PAGES	19a. NAME OF RESPONSIBLE PERSON
a. REPORT	b. ABSTRACT	c. THIS PAGE			19b. TELEPHONE NUMBER (*Include area code*)
Unclassified	Unclassified	Unclassified	UU	36	John Schmidt 410-278-5510

Standard Form 298 (Rev. 8/98)
Prescribed by ANSI Std. Z39.18

Contents

List of Figures

List of Tables

INTENTIONALLY LEFT BLANK.

1. Introduction

Currently, large-caliber guns require a heavy mount to absorb the recoil. However, the emphasis in the U.S. Army is now on lightweight and deployable vehicles. The Rarefaction wAVE guN (RAVEN) was invented by Kathe (*1*) to substantially reduce the recoil and, hence, the mass of the system that absorbs the recoil, while minimally reducing the projectile velocity. This is accomplished by venting the breech through an expansion nozzle during the firing cycle. If the timing is done correctly, the rarefaction wave from the venting will not reach the projectile until muzzle exit. Therefore, the projectile does not know that the vent has opened.

In a previous report, a one-dimensional (1-D) code Rarefaction wAve Recoil (RAR) was developed to model the interior ballistics and recoil of the RAVEN (*2*). The model was validated against the 35-mm gun data. Currently, a 105-mm demonstrator RAVEN gun showing significant differences from the 35-mm gun design is being designed.

The code has been updated for both gun designs. In the process, a number of small improvements have been made. Also, there has been one significant change in the behavior of the nozzle.

In this report, the new version of the code is applied to the 35-mm data. One change in the input to the code is made to improve the agreement in the recoil velocities. The code is then used to predict the behavior of the proposed 105-mm demonstrator.

2. The 35-mm RAVEN Fixture

Figure 1 shows an assembly drawing of the 35-mm RAVEN. The starting point is a 35-mm KD series antiaircraft gun (*3*). The chamber diameter is 55 mm, so there is substantial chambrage. The propellant is a proprietary single-perforated, deterred grain.

The moving breech/piston is in the shape of a delta wing. The breech is held into place by a shear plug (figure 2) designed to shear at 220 MPa. The chamber plug determines how far the piston moves before opening the vent into the expansion nozzle. There were four different recoil distances to venting—early, nominal, intermediate, and late.

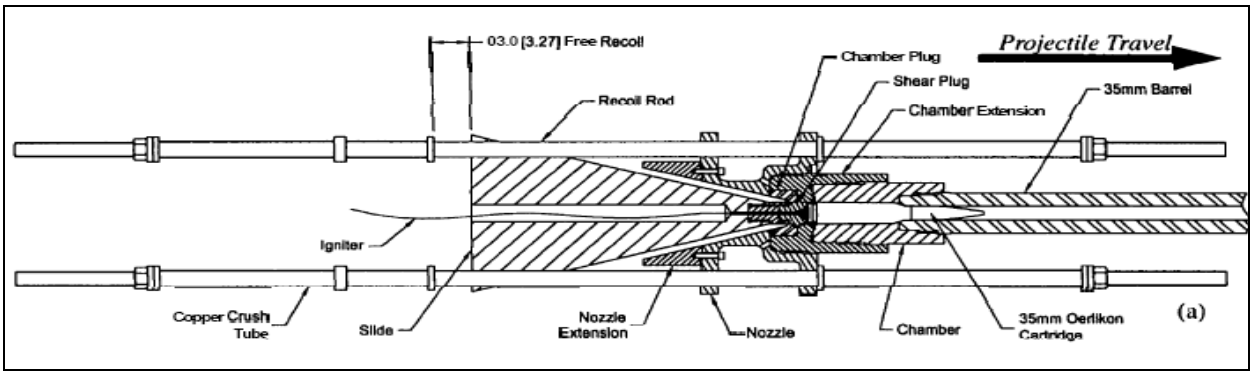

Figure 1. RAVEN 35-mm assembly drawing.

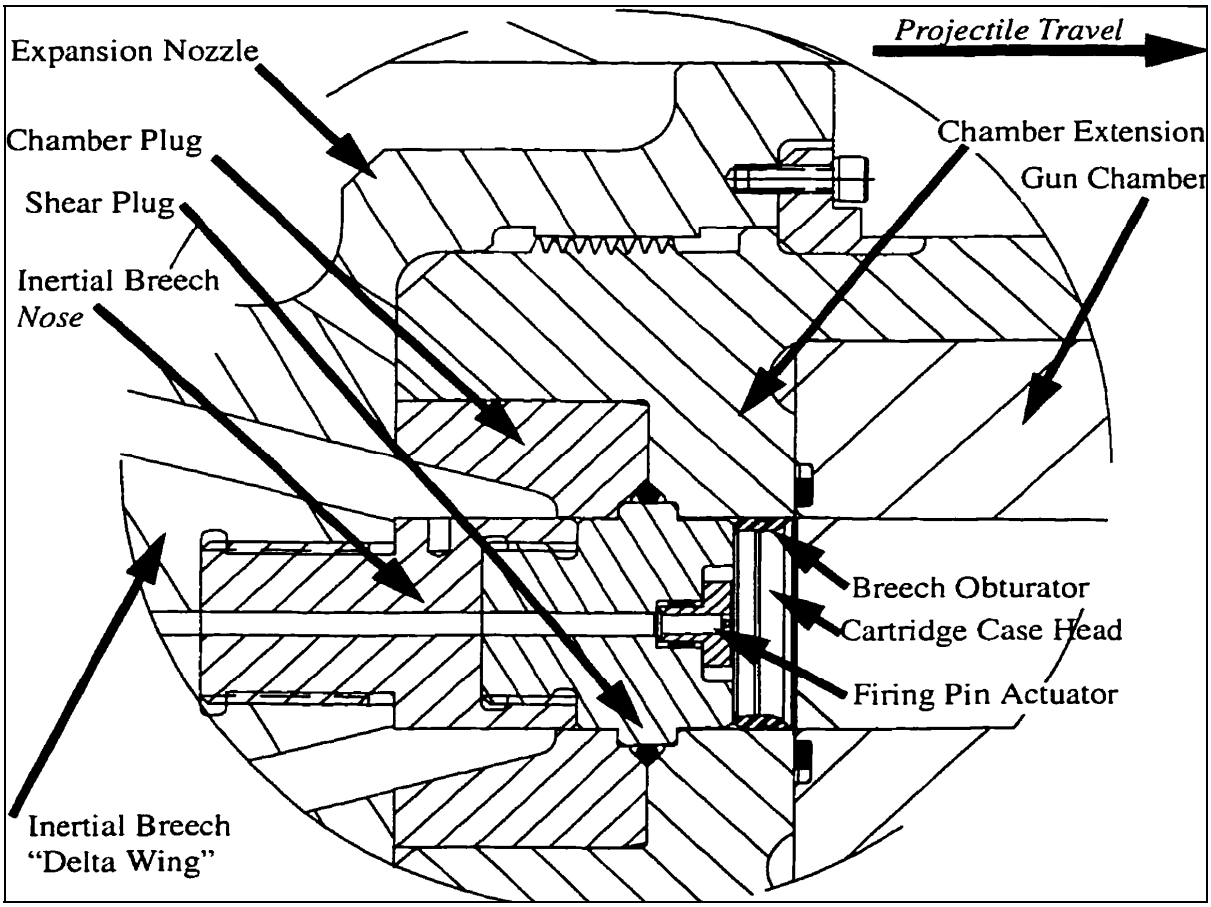

Figure 2. RAVEN 35-mm internal working.

Two different pistons (light and heavy) were used in the tests with venting. A piston without a vent was also used. A T-bar replaced the delta wing. Finally, the fixture was shot in a closed-breech configuration. The heavy piston was used, but with a steel shear plug instead of an aluminum shear plug. As a result, the piston did not move. Each configuration had a different recoiling mass.

A piston can move freely for 83 mm until it impacts two copper crush tubes (figure 1). The tubes are designed to bring the piston to a halt within 30 ms. The free recoil velocity is the velocity of the tube/piston system after the velocities equilibrate. The system utilizes a free recoil mount. The mount provides 25.9 mm of travel forward and 25.4 mm of travel rearward. The free recoil velocity is measured after the tube and the piston equilibrate and before the gun hits the ring-spring recoil arrestors.

3. The 105-mm RAVEN Fixture

The proposed 105-mm demonstrator is based on a modified cased telescope ammunition automatic Colt pistol cartridge. The projectile has a long boat tail extending almost to the breech. The charge is JA2 stick propellant. Figure 3 shows a preliminary design (*4*) where the breech is replaced by a piston with one of six spindles on the end. The spindle initially seals the breech. Unlike the 35-mm gun, there is no shear plug. The piston is initially held in place by recuperators exerting a small forward force (see section 5.4). Spindle A (left) takes the longest time to open the vent. The other spindles are cut away to open the vent sooner.

The demonstrator has a split nozzle. The inside part of the nozzle is attached to the gun. The outside part of the nozzle is attached to the piston (not shown). As the piston moves backwards, the nozzle becomes longer.

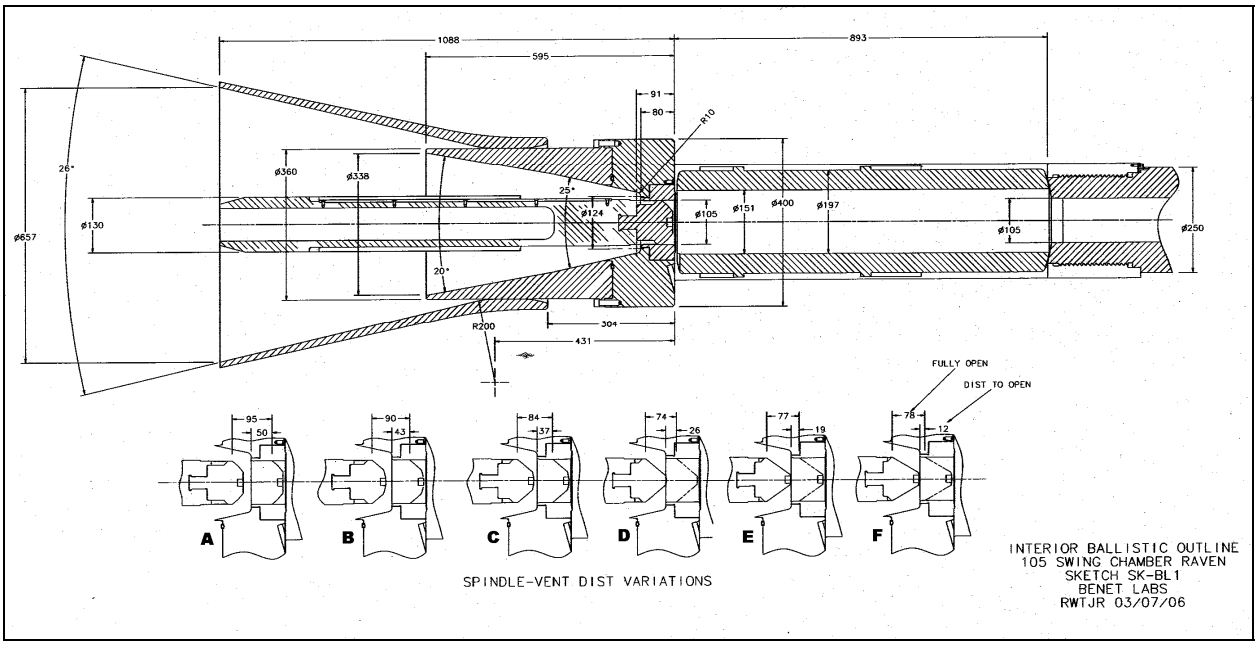

Figure 3. RAVEN 105-mm design.

The piston is stopped by recoil brakes. Unlike the 35-mm gun, the piston is decelerated to the mount instead of the gun. Recuperators return the piston to the initial position. The gun will move forward at a slow velocity and is stopped with forecoil pads.

4. The 35-mm RAVEN Code

A 1-D code RAR was developed to model the interior ballistics and recoil of the RAVEN. This section quickly reviews the code as described in much more detail in the previous report (*2*). The next section describes modifications of the code.

The basic approach is a finite volume Arbitrary Lagrangian-Eulerian (ALE) code. The computational domain is split into volumes. The scalar quantities (pressure, temperature, etc.) are assumed constant inside each volume, with a jump at the boundaries of the volume. The velocities are defined on the boundaries of the finite volumes (vector grid points). For a 1-D code, the velocities are only axial. Radial and tangential velocities in the chamber and nozzle are ignored.

4.1 Nonconformal Grid

The RAR code requires a nonconformal grid. A 1-D grid (with area changes) is set up from the nozzle end to the muzzle end. The grid does not move. The projectile and piston will move through the grid. The scalar control volumes are numbered from i = 1 (nozzle end) to i = nx – 1 (muzzle end). The vector grid points are numbered from i = 1 to i = nx. For instance, the pressure in the scalar control volume i (p_i) is between the velocities v_i and v_{i+1}. The point where the breech would be located in a standard gun is usually assigned the axial value 0. The points in the chamber and gun tube have positive values, and points in the nozzle have negative values.

The input includes the shape and initial location of the piston and projectile. A subroutine splits each scalar control volume into propellant volume (gas and unburnt propellant grains) and metal volume (piston or projectile). It also splits the areas at the vector grid points (finite volume boundaries) into propellant and metal areas.

Initially, the propellant grains are spread evenly between the piston and the projectile, as well as the primer (assumed to be already gas). Air is inserted at atmospheric pressure and temperature before the piston and after the projectile.

4.2 Motion of the Projectile/Piston/Gun

There are three moving parts in the 35-mm RAVEN—the projectile, piston, and gun. Input to the code includes the projectile resistance pressure p_j as a function of projectile travel, the piston resistance pressure p_s as a function of piston travel, and the gun resistance pressure p_g

as a function of gun travel. The projectile resistance is from the force required to engrave the projectile rotating band and the friction down the tube. At first, the shear plug causes piston resistance; later, it's from the crush tubes. The gun resistance is caused by friction between the gun and the mount. Note that for computing the projectile and piston resistance, the projectile and piston travels are relative to the position of the gun.

There are four cases. Before the chamber pressure reaches the projectile shot start pressure or the piston shear pressure, none of the masses move. Normally, the projectile will start to move before the piston. The projectile moves forward, and the piston/gun recoils as a unit. Note that this occurs before the piston shears and also after the crush tubes bring the piston to a halt. It is possible for the piston to shear before shot start pressure. In this case, the projectile and gun will move forward as a unit, and the piston will move backward. This is not expected to occur in practice. Finally, all three masses can move independently.

Consider the general case where all three masses move independently. Let A_i be the area of the nozzle/chamber/tube at the i'th vector grid point. Let AM_i be the area of metal (piston or projectile) at this point and AP_i be the area that is not blocked by metal. The force on the projectile will be as follows:

$$F_j = \sum p_i (AM_{i+1} - AM_i) - p_j A_{nx} \ , \tag{1}$$

where the summation is taken from the left to the right of the projectile. This includes the force on a general boat tail, the force due to the air being compressed in front of the projectile, and the resistance pressure.

Figure 4 illustrates how this formula works. The figure shows a short projectile with a simple boat tail and a coarse grid. Consider the scalar control volume between 12 and 13 cm. The pressure is assumed to be constant in a control volume. This pressure acts on the left side of the projectile and on the slanted top up to 13 cm. The axial area the pressure acts on is the area at 13 cm. According to equation 1, the pressure acts on the area at 13 cm minus the area at 12 cm. Since the projectile area at 12 cm is 0, the formula is correct. Between 13 and 14 cm, the pressure acts on the slanted surface. The projection in the axial direction is just the area at 14 cm minus the area at 13 cm. This continues to the base of the projectile.

In the cylindrical part of the projectile, the metal area is the same at both ends of the control volumes. There is no force from these volumes. Last, consider the control volume between 21 and 22 cm. The area at 22 cm minus the area at 21 cm equals the negative of the tube area. From equation 1, the pressure at the right of the projectile exerts a backwards force on the projectile.

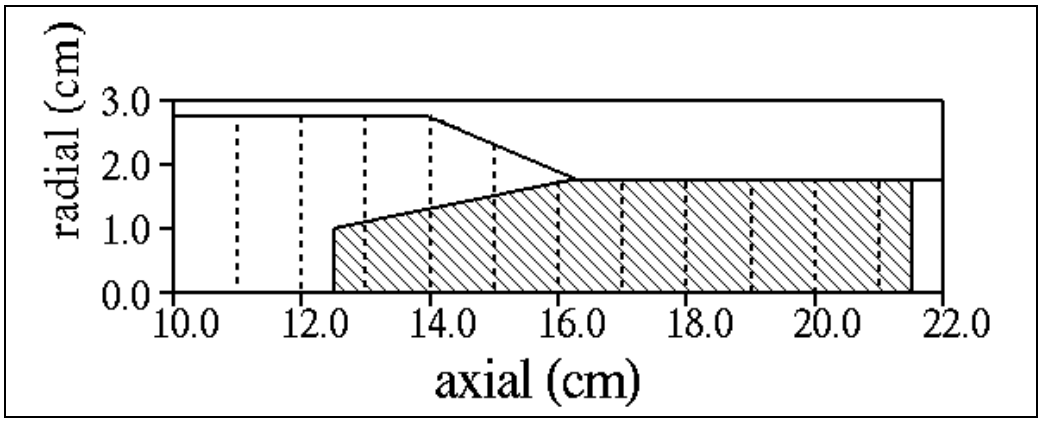

Figure 4. Numerical grid around a projectile with a boat tail, chamber (line), vector grid (dot), and projectile (shaded).

Let A_p be the area at the right end of the piston (breech area). Let p_a be atmospheric pressure, which is assumed to be 0.1 MPa. Then, the force on the piston will be as follows:

$$F_s = \sum p_i (AM_{i+1} - AM_i) + p_a AM_1 - p_s A_p \ . \tag{2}$$

The summation is from the left to the right of the piston. The resistance pressure is applied to the breech area. If the piston extends past the end of the computational domain, the new term $p_a AM_1$ takes into account the atmospheric pressure on the left of the piston. A similar term is not necessary for the projectile because at muzzle exit, the pressure on the base of the projectile is much higher than atmospheric pressure. This is not true for the piston. Before projectile exit, as the chamber pressure drops, the nozzle becomes overexpanded. The pressure at the end of the nozzle is under atmospheric pressure. The pressure at the left end of the piston may not be negligible.

The force on the gun is given by the following:

$$F_g = \sum \max (p_i , p_a)(A_i - A_{i+1}) - p_a (A_1 - A_{nx}) - p_s A_p + p_j A_{nx} \pm p_g A_p \ . \tag{3}$$

The summation is over the entire computational domain. In the nozzle, the pressure is the maximum of the local and atmospheric pressures. When the nozzle is badly overexpanded, the flow will separate. If the pressure in the nozzle is under atmospheric pressure, the formula assumes the flow has separated and atmospheric air has entered the nozzle (first term on the right-hand side). This correction makes a noticeable difference in the free recoil velocity. Unfortunately, this correction turns out to be wrong (see section 5.2). The second term is the pressure on the outside of the gun. This has a substantial effect on the recoil velocity. The third term is the effect of the piston resistance. If there is piston resistance, the piston will pull the gun backwards. The fourth term is the effect of projectile resistance. Finally, the last term is the effect of the friction between the gun and the mount. This force acts opposite the motion of

the gun. For the sake of consistency, the gun friction force is calculated as a pressure multiplied by an area. There is not a natural area for the force between the gun and the mount so, arbitrarily, the piston area is used.

The problem is solved in the lab framework. When the gun moves, the grid moves with the gun. Since the basic implementation is an ALE code, this is easy to do.

4.3 Vent Opening

When the piston travels a specified distance, the vent rapidly opens into a 30° nozzle (see figure 2). This is approximated in the code as a jump condition in the radius. Figure 5 shows the grid for an early open case. The dotted lines indicate the vector grid points. The scalar control volumes are between the dotted lines. The vent opens at –4.888 cm, where the radius jumps from 2.75 to 3.1145 cm. The area at the jump is computed using the smaller diameter (dotted line). The volume of the scalar control volume to the right is computed using the smaller diameter, and the volume of the scalar control volume to the left is computed using the larger diameter.

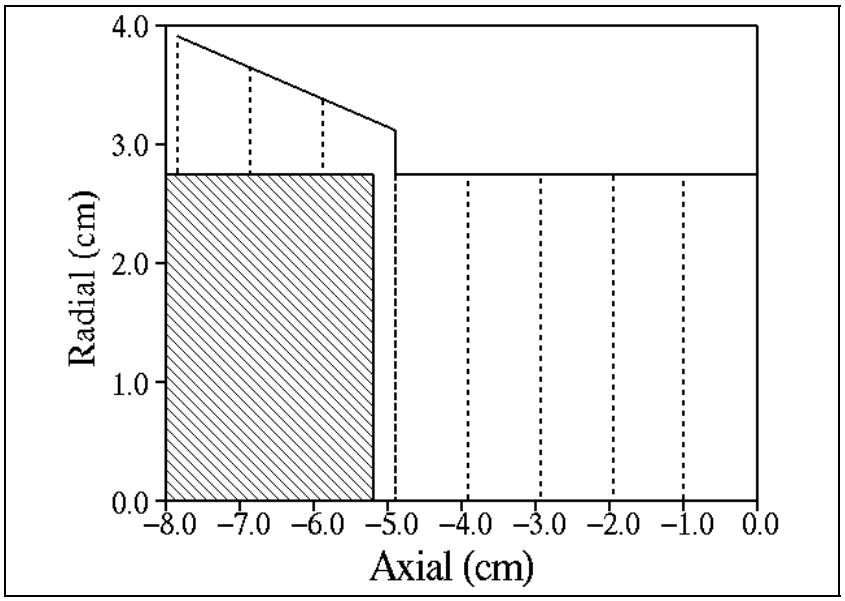

Figure 5. Numerical grid at vent opening, nozzle (line), vector grid (dot), and piston (shaded).

There is an additional complication: in figure 5, the piston has just opened the vent. Consider the scalar control volume at the right end of the piston. The area at the right is the chamber area, and the area at the left is the area between the piston and the nozzle. However, the physical minimum flow area is the space between the corner of the piston and the end of the chamber.

If this is ignored, the vent appears to open too quickly. As soon as the piston just clears the jump, the code thinks there is a large opening between the chamber and the nozzle. To fix this,

the area between the right corner of the piston and the jump point is computed. The area at the left of the control volume is reduced to the minimum of the normal area and this new area. Material can flow into the control volume as soon as the piston passes the jump point, but it cannot pass quickly into the nozzle.

4.4 Boundary Conditions

Consider the flow out of the gun tube. When the projectile first exits, the flow will normally be supersonic. In this case, simple extrapolation is used, i.e., $v_{nx} = 2\ v_{nx-1} - v_{nx-2}$. The flow quickly becomes subsonic. The flow out of the tube is assumed to be a steady-state isentropic flow (*5*). If the outflow velocity is larger than the local sound speed, it must be lowered to the sonic velocity (choked flow). The flow will be choked for most of the blow-down phase.

Consider the flow out of the nozzle. Once into the expanding nozzle, the flow will become supersonic. If extrapolation is used to get the velocity at the nozzle exit, the gun will continue to empty until the pressure in the gun is well under atmospheric pressure. The flow cannot be revised in a 1-D code.

In reality, the flow will separate when the pressure becomes low enough. To roughly approximate this in the 1-D code, the pressure at the nozzle exit is tracked. If the flow is supersonic and the pressure in the first control volume is greater than atmospheric pressure, the velocity is extrapolated ($v_1 = 2\ v_2 - v_3$). If the pressure in the first control volume is less than atmospheric pressure, the normal momentum equation is used. There will be flow into the nozzle. The material outside the nozzle is assumed to be air at atmospheric pressure and temperature. This is a crude approximation to separated flow. A better approximation is discussed in section 5.2.

4.5 Combustion

The combustion model is copied from IBHVG2 (*6*). At time 0, the primer is assumed to be already combusted and the gas spread evenly through the gun. The propellant grains are also spread evenly between the piston and the projectile. The burn rate of each grain is based on the mean pressure in the gun (average pressure between the right end of the piston and the left end of the projectile). The burn rate times the time step gives the depth of propellant burnt. A form function gives the surface area as a function of the amount of each grain burnt. The propellant is assumed to move with the gas (infinite drag). The code has fewer capabilities than the 1-D code XKTC (*7*). However, if the charge is well behaved, this level of approximation is adequate.

A new form function is required for the single-perforated, deterred grains in the 35-mm gun. To create a deterred grain, the deterrent is diffused into a grain, implying a gradual transition from the outer to inner layer. In practice, however, the deterrent concentration is nearly constant in the deterred layer and falls off sharply at the boundary line. The grain is modeled as if there is a sharp boundary between the outer and inner layers and the depth of the deterred layer is constant.

This led to the introduction of two new form functions. The outer layer form function behaves like a normal single-perforated grain, except a depth of the deterred layer is also entered. When that depth is reached, the outer layer is gone and the inner layer starts to combust. The initial dimensions of the inner layer are obtained from the dimensions of the initial grain and the depth of the deterred layer.

5. Modification of the RAVEN Code

There have been a number of changes in the RAVEN code since the previous report (*2*). Most of the updates have only minor effects. Two changes have a noticeable effect on the 35-mm RAVEN modeling (sections 5.1 and 5.2). Other changes are made to model new features of the 105-mm demonstrator (sections 5.3–5.5).

5.1 Heat Transfer to the Tube

In the earlier version of the code, the heat loss to the gun tube was computed using a pipe flow correlation. The resulting rise in the tube temperature was not computed.

For the demonstrator, the tube temperature is interesting, particularly for a multishot scenario. The temperature of the wall is computed, assuming a polynomial fit of the radial temperature in the wall (see Gough and Zwarts [*8*] for details). The heat flow is based on the difference between the gas and wall temperatures. Since the wall becomes hotter during the firing cycle, the heat transfer is somewhat less than before. The muzzle velocity shows a small but noticeable increase.

5.2 Nozzle Exit Conditions

A normal rocket operates at a constant chamber pressure. The rocket nozzle is ideal if the pressure drops to atmospheric pressure at the end of the nozzle, resulting in the maximum thrust. If the nozzle is shorter than an ideal nozzle (underexpanded), the force exerted on the end of the ideal nozzle is lost and the thrust is reduced. If the nozzle is longer than an ideal nozzle (overexpanded), the flow will separate from the nozzle. The pressure past the end of the ideal nozzle is no more than atmospheric pressure, and the additional nozzle length is not useful.

For a RAVEN gun, the pressure in the chamber is definitely not constant. For most of the recoil phase, the nozzle is very badly overexpanded. The question is how to model a transient, overexpanded nozzle.

In the previous version of the code, it was assumed that when the flow separated, gas flowed out the middle of the nozzle but air flowed in at the edges of the nozzle. The pressure on the inside of the nozzle was the maximum of the computed pressure and atmospheric pressure (see equation 3), resulting in an incorrect assumption.

As a partial check of this assumption, a simplified version of the RAVEN code was written with a two-dimensional nozzle. Simulations showed that the pressure and velocity stayed close to constant across the nozzle, even when badly overexpanded. Assuming atmospheric pressure was 0.1 MPa, the pressure at the nozzle exit went down to 0.01 MPa before the flow backed up into the nozzle.

Further research indicated that a steady-state rocket was expected to flow full until the exit pressure dropped to 0.4 times the outside pressure. At this point, the flow reversed. The separation point is where the flow into the nozzle meets the flow trying to come out of the nozzle. The idea of flow going out the center of the nozzle and in at the edges was unrealistic.

Therefore, the code was modified. The exit velocity is found by extrapolation until the pressure at the end of the nozzle equals 0.01 MPa. At this point, the code instead computes the exit velocity, assuming a pressure of 0.1 MPa just outside the nozzle. Simulations indicate that the exact pressure used to convert from extrapolation to calculation is not important as long as the pressure is under 0.1 MPa. If the change is made at a higher pressure, the velocity and pressure profiles are the same except at the very end of the nozzle. The flow cannot move into the nozzle against the force of the outflow. It is only when the exit pressure drops near 0.01 MPa that the outside air starts to really penetrate the nozzle. Since the model is transient rather than steady state, the pressure at the exit drops below the 0.04 MPa expected from a steady-state solution.

When the pressure in the nozzle is below atmospheric pressure, the air outside the nozzle then exerts a rearward force on the gun. For the 35-mm simulations, this results in a noticeable increase in the recoil velocities.

5.3 Split Nozzle

The preliminary demonstrator design has a split nozzle (figure 3). The inner section is attached to the gun, and the outer section is attached to the piston. Figure 6 shows the initial configuration and the configuration after the piston has moved 10 cm.

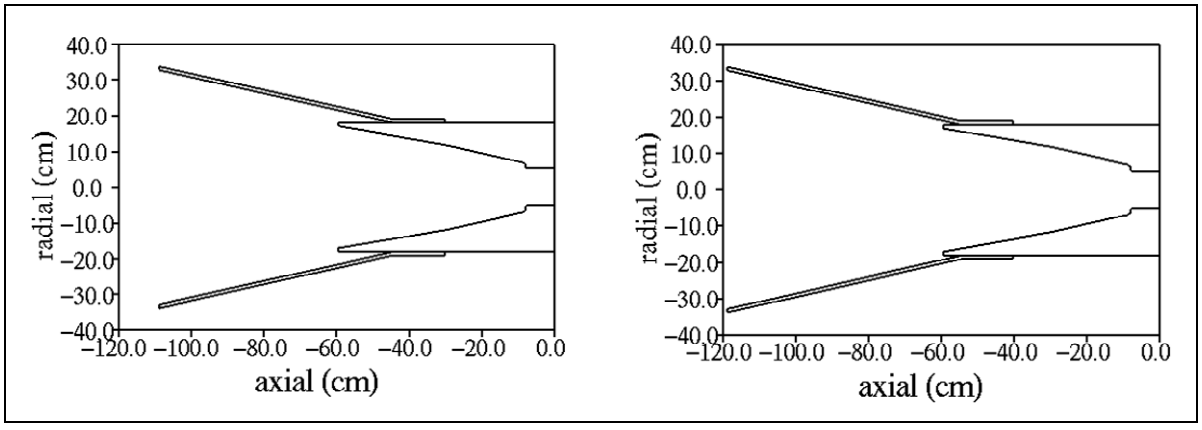

Figure 6. Split nozzle and initial configuration (left); piston has moved 10 cm (right).

Figure 7 shows the initial grid at the point where the nozzles overlap (not to scale). There is a jump in radius at the end of the inside nozzle. The volume over the inner nozzle and under the outer nozzle is ignored. There is no practical way to represent this in a 1-D code, and the volume is relatively small.

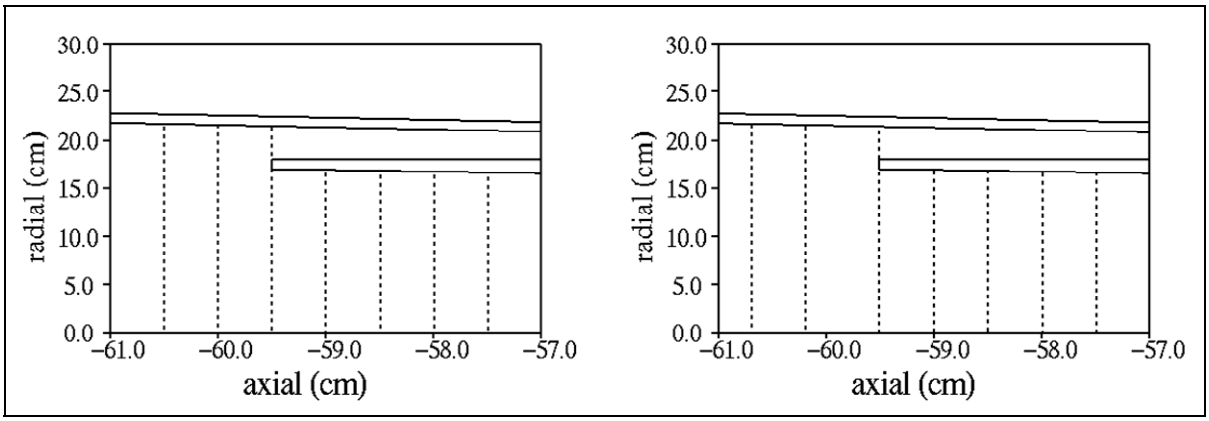

Figure 7. Grid near nozzle join, initial grid (left), and grid just before addition of a grid point (right).

The input file now includes a parameter inozz, which is the vector grid point where the nozzles meet. If inozz = 1, the entire nozzle is attached to the gun (previous case). Otherwise, the nozzle from I = 1 to i = inozz is attached to the piston, and the rest of the nozzle is attached to the gun. The shapes of both nozzle parts are entered as tables of diameter vs. distance.

As the integration proceeds, vector grid points $\geqq$inozz move with the gun, and vector grid points <inozz move with the piston. Unlike the 35-mm simulations, this case requires a simple adaptive grid. The control volume just to the left of the join becomes larger. All the other control volumes remain the same. When the length of this control volume becomes 50% larger than the length of the adjacent control volume, it is split into two control volumes. All the control volumes to the right of inozz are renumbered up one. The control volume just to the left of inozz is split at the 2/3 points. That is, the original grid has 0.5-cm spacing. When the control volume just to the left of inozz has increased to a length of 0.75 cm, it is split into a control volume 0.5 cm long (to the left) and a control volume 0.25 cm long (to the right). The procedure is repeated as necessary through the integration.

5.4 Recoil Brakes and Recuperators

For the 35-mm gun, the piston has to break the shear plug to start moving. Later, the piston is slowed by the crush tubes. The piston resistance is read in as a table of pressure (MPa) vs. piston travel (centimeters). The resistance force is the pressure times the piston area.

For the 105-mm demonstrator, the piston is instead decelerated regarding the mount. The piston is primarily stopped by the recoil brakes. The recoil brakes are a viscous damper in which fluid is forced through an orifice varying in size according to the stroke. The mechanism is a rod of varying diameter which passes through the orifice. The input is a table of a parameter K (newton-squared seconds/squared centimeters) vs. the piston travel (centimeters). The recoil brake force is then K times the piston velocity squared (N = 0.01 MPa-cm^2). The recoil brakes only function if the piston is moving rearward.

The recoil brakes will not bring the piston to a complete halt. As the piston slows down, the recoil brake force becomes very small. The piston is brought to a complete halt and then returned to the original position by recuperators (gas springs). The recuperator resistance is read in as a table of pressure (megaPascals) vs. piston travel (centimeters). The actual force is the pressure from the table times the piston area. When the piston has returned to its original position, the piston is stopped.

The gun resistance is read in as a table of pressure (megaPascals) vs. gun travel (centimeters). Somewhat arbitrarily, the force on the gun is the pressure from the table times the piston area. The force may be from to friction between the gun and the mount, or it may be a designed force such as forecoil pads. In the new version of the code, all three forms of piston resistance are implemented. Any or all of the tables can be set to 0 in the input file.

5.5 Combustion

The combustion model used for the 35-mm gun was copied from IBHVG2 (*6*). At time 0, the primer is assumed to be already combusted and the gas spread evenly through the gun. The charge is also spread evenly between the breech and the projectile. The burn rate of each grain is based on the mean pressure in the gun (average pressure between the right end of the piston and the left end of the projectile). The burn rate multiplied by the time step gives the depth of propellant burnt. A form function gives the surface area as a function of the amount of each grain burnt. The propellant is assumed to move with the gas (infinite drag) and therefore remains evenly dispersed.

For the 105-mm gun, the primer is localized near the breech. There are four different types of stick propellant located in different parts of the chamber, designed to fit around the boat tail. Some of the capabilities of the 1-D code XKTC (*7*) are implemented. The primer and the various types of propellant can be located in specified axial regions of the gun. The primer can be set to combust at a constant rate for a specified period of time. The propellants still combust according to the mean pressure and move with the gas. The code has fewer capabilities than XKTC but should be adequate for a well-behaved charge.

6. The 35-mm RAVEN Simulations

The measured data for the experiments consists of pressure profiles, muzzle velocity, and gun travel. The recorded pressures were known to drift. Therefore, no attempt was made to match the maximum chamber pressure. When possible, the shape of the pressure profile, the time the vents open (when applicable), the muzzle velocity, and the free-recoil velocity were the matched values.

The maximum pressures fell into two groups, which were widely separated. The muzzle velocities were strongly correlated with the pressures, indicating that this was a real effect. Lacking other information, this was possibly from the propellant charge.

The gun charge was a proprietary single-perforated, deterred grain. The chemical constituents were supposed to be similar to M1 propellant (*1*). Given only this information, a combustion model was created by trial and error. For the high-pressure group, the outer layer was assumed to burn 10% faster than for the low-pressure group. An estimate of the projectile shot start, engraving force, and bore friction was made by Kathe (*1*). Lacking other information, this profile was used for the projectile resistance.

The calculated free-recoil velocity for the closed-breech gun was initially substantially high. To correct this, a constant gun resistance pressure of 4 MPa was included in the model. The resistance force was then 4.0 MPa × the breech area (cm^2) = 95 MPa-cm^2 = 9500 N-s.

The shear plug was designed to fail at 220 MPa. The shear web was 1.0 cm long. The resistance pressure was assumed to drop rapidly when the shear plug failed and then drop gradually to 0 at 1 cm of travel. At 8.3 cm of travel, the piston hit the crush tubes. Each tube was designed to have a generally constant crush load of 55,000 N-s (*1*). For both tubes, the resistance pressure would be 46.3 MPa. The experimental data indicated that the crush tube load was not repeatable. A value of 40 MPa was previously used to better agree with the venting data.

Primarily due to the correction in the nozzle pressure (section 5.2), the calculated recoil velocities for the venting cases were uniformly high. The piston resistance profile was modified to improve the agreement (see table 1). This caused less agreement for the vent opening times (see section 6.3).

6.1 Closed-Breech Cases

Consider first the closed-breech cases. The results should be the same as the baseline 35-mm gun results. The baseline gun has a muzzle velocity of 1175 m/s and a maximum chamber pressure of 383 MPa (*9*).

Table 1. Piston resistance profile.

Piston Travel (cm)	Old Resistance Pressure (MPa)	New Resistance Pressure (MPa)
0.0	220	220
0.001	110	50
1.0	0	0
8.3	0	0
8.4	40	46.3
>8.4	40	46.3

Table 2 summarizes the results. All three closed-breech firings belong to the low-pressure group. The maximum experimental chamber pressures are all much lower than expected, while the calculated maximum pressure is reasonable. Except for the first experiment, the experimental and calculated muzzle velocities are as expected. For all three shots, the measured gun travels are virtually identical. The gun travels must be differentiated numerically, adding uncertainty to the recoil velocity results. The recoil velocities are in excellent agreement since the friction between the gun and the mount was chosen to obtain agreement.

Table 2. Closed-breech gun: comparison of experimental and model results.

		Pressure (MPa)		Muzzle Velocity (m/s)		Recoil Velocity (m/s)	
Configuration	Shot No.	Experimental	Model	Experimental	Model	Experimental	Model
Closed breech	2-1-1	348	398	968	1175	2.69	2.67
—	2-1-2	334	398	1184	1175	2.69	2.67
—	2-1-3	346	398	1166	1175	2.65	2.67

6.2 Nonventing Cases

There are two shots with the nonventing moving breech where the gun motion is recorded. Shot 2-9-3 is in the low-pressure group, and shot 2-9-4 is in the high-pressure group. The breech moves backward, but there is no venting (no nozzle). This separates the effect of the moving breech from the effect of venting gas out the back.

When the breech starts to move (at 220 MPa), the gun initially moves forward because of the large chambrage in the gun. When the piston hits the crush tubes, the gun is gradually stopped and dragged backward. The two recorded gun travels are quite different, indicating that the crush tubes are not repeatable. However, the details have very little effect on the recoil velocity. All that is necessary is that the piston momentum be transferred to the gun before the gun hits the ring-spring arrestors (not in the model).

The friction between the gun and the mount has very little effect on the moving-breech cases. For the closed-breech cases, the gun always moves backwards. The friction always slows down the recoil. For the other cases, the gun moves forward and then backward. The frictional effect

when the gun moves forward comes close to canceling out the frictional effect when the gun moves backward. Table 3 summarizes the results. The calculated recoil velocities are a little less than the experimental recoil velocities.

Table 3. Nonventing gun: comparison of experimental and model results.

Configuration	Shot No.	Pressure (MPa)		Muzzle Velocity (m/s)		Recoil Velocity (m/s)	
		Experimental	Model	Experimental	Model	Experimental	Model
Nonventing	2-9-3	337	389	—	1133	2.35	2.26
	2-9-4	401	450	1135	1166	2.43	2.30

6.3 Light-Piston Cases

For the vent-opening cases, the model includes a 30° expansion nozzle. The diameter at the exit plane of the nozzle is about 23.65 cm. Table 4 summarizes the results. Again, the model pressures are higher than the experimental pressures. The muzzle velocity was not measured for two shots. In general, the muzzle velocities are also in good agreement. There is not much change in the muzzle velocity as the vent opening time is changed. The recoil velocities are also in good agreement. The greatest reduction in recoil velocity occurs when the piston opens early. This allows the nozzle to generate thrust for a slightly longer period of time.

Table 4. Light piston: comparison of experimental and model results.

Configuration	Shot No.	Pressure (MPa)		Muzzle Velocity (m/s)		Recoil Velocity (m/s)	
		Experimental	Model	Experimental	Model	Experimental	Model
Light early	2-6-1	408	434	1107	1126	1.29	1.43
	2-6-2	404	434	1129	1126	1.45	1.43
	2-6-3	328	380	1064	1092	1.36	1.35
Light nominal	2-5-1	397	434	1131	1130	1.42	1.50
	2-5-2	397	434	1130	1130	1.53	1.50
	2-5-3	408	434	1116	1130	1.51	1.50
Light inter	2-7-1	340	380	—	1098	1.39	1.59
	2-7-2	343	380	1093	1098	1.52	1.59
	2-7-3	331	380	1070	1098	1.42	1.59
Light late	2-8-1	342	380	1085	1099	1.68	1.73
	2-8-2	385	434	—	1132	1.68	1.81
	2-8-3	328	380	1071	1099	1.75	1.73

Figure 8 shows the chamber pressure for an early vent opening case. There is a sharp change in the slope between 2 and 3 ms, corresponding to the opening of the vent. The old simulation matched the time of the slope change slightly better. If the old piston resistance profile (table 1) is used with the new version of the code, the vent opening time is more accurate, but the recoil velocities are uniformly high. We chose to get a better match to the recoil velocities instead of the pressure profile slope change.

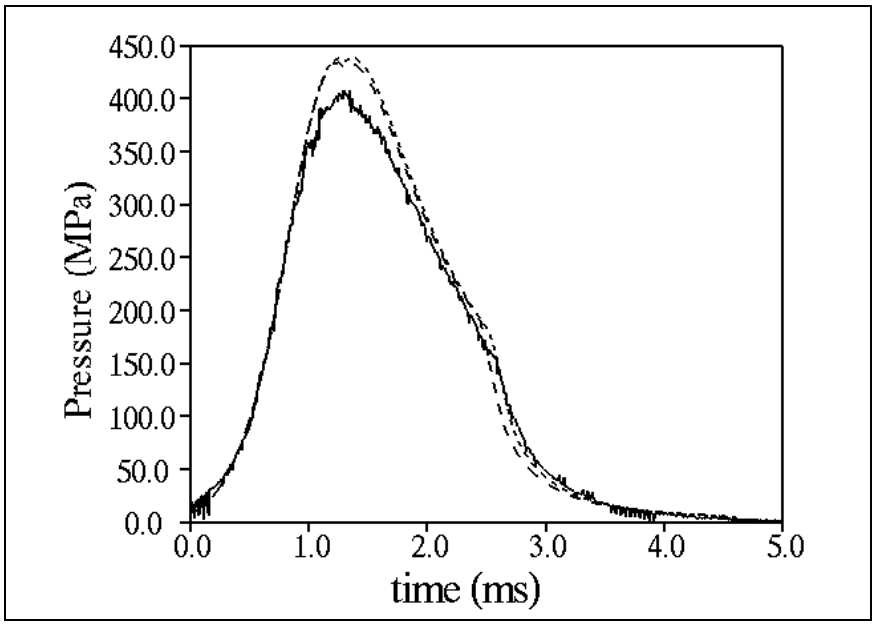

Figure 8. Shot 2-6-2: light piston, early vent, high-pressure group; gauge P1 (line), previous simulation (dot), and new simulation (dash).

6.4 Heavy-Piston Cases

The heavy piston does not move as rapidly at early times. This causes a slightly higher chamber pressure and muzzle velocity than the equivalent light-piston cases. On the other hand, for a particular opening distance, the recoil reduction is less. Table 5 summarizes the results. The agreement is about as good as for the light-piston cases.

Table 5. Heavy piston: comparison of experimental and model results.

Configuration	Shot No.	Pressure (MPa)		Muzzle Velocity (m/s)		Recoil Velocity (m/s)	
		Experimental	Model	Experimental	Model	Experimental	Model
Heavy early	2-3-3	390	449	1164	1164	1.77	1.84
	2-3-4	319	387	—	1131	1.70	1.77
	2-3-5	402	449	1131	1164	1.78	1.84
Heavy nominal	2-2-1	382	449	1128	1170	1.76	1.92
	2-2-2	401	449	1165	1170	1.75	1.92
	2-2-3	330	387	1128	1131	1.70	1.84
	2-3-1	409	449	—	1170	1.93	1.92
	2-3-2	409	449	—	1170	1.88	1.92
Heavy inter	2-4-1	413	449	1143	1165	2.05	2.08
	2-4-2	418	449	1155	1165	1.98	2.08
	2-4-3	413	449	1194	1165	2.02	2.08

6.5 Parametrics

In the experiments, the masses are different for the four cases (closed breech, nonventing, light piston, and heavy piston). Now that because the code has agreed with the experimental data, more direct comparisons are possible.

As a baseline, arbitrarily consider the heavy piston. The code is run with a closed breech and a nonventing piston but with the gun mass (297.6 kg) and piston mass (35.9 kg) from the heavy-piston cases. Then, the code is run for a venting piston with various opening times. The starting point is the early-open vent, where the vent opens at 4.888 cm of travel and the diameter jumps from 5.5 to 6.229 cm. The distance to the vent opening is varied. The diameter jump at the opening remains the same, as does the nozzle after the opening.

When comparing the experimental data, a constant friction force is assumed between the gun and the mount. The friction has more of an effect on the closed-breech simulations (gun always moves rearward) than on the other cases (gun moves forward and then rearward). To see the effect of a moving breech and venting more clearly, the friction is assumed to be 0 in this section.

Table 6 shows the results. Just by having a moving breech (nonventing piston), the pressure drops slightly and the muzzle velocity drops 3.7%. The recoil is slightly less because of the lower performance. For the venting cases, the distance (centimeters) until the vent opens is given. If the vent opens after 4 cm, there is a negligible drop in muzzle velocity and a 50% drop in the recoil, compared to the nonventing case. The recoil can be decreased even more if a lower muzzle velocity is acceptable.

Table 6. Heavy piston: no gun resistance and comparison of simulations.

Configuration	Pressure (MPa)	Muzzle Velocity (m/s)	Recoil Velocity (m/s)	Momentum (N-s)
Closed breech	398	1175	3.14	1049
Nonventing	388	1132	3.03	1009
Vent 5.0	387	1131	1.66	554
Vent 4.0	387	1130	1.51	503
Vent 3.0	387	1126	1.31	437
Vent 2.0	387	1093	1.04	347
Vent 1.0	387	992	0.64	214

During the gun blow down, the pressure in the nozzle will fall below atmospheric pressure. The nozzle will then accelerate the gun rearward instead of forward. To check this effect, the runs in table 6 are redone with the length of the nozzle cut in half. The nozzle angle is kept the same, so the exit diameter is smaller.

Table 7 shows the results. Consider the cases where the vent opens after 5 or 4 cm of travel (relatively late). Reducing the size of the nozzle actually leads to a very small decrease in the recoil. For the other three cases (opens earlier), there is a slight increase in the recoil. The differences are not significant. The optimum nozzle size depends on the particular case of interest. However, it is clear that the nozzle used in the experiments is larger than necessary.

Table 7. Heavy piston: no gun resistance, short nozzle, and comparison of simulations.

Configuration	Pressure (MPa)	Muzzle Velocity (m/s)	Recoil Velocity (m/s)	Momentum (N-s)
Closed breech	398	1175	3.14	1049
Nonventing	388	1132	3.03	1009
Vent 5.0	387	1131	1.65	551
Vent 4.0	387	1130	1.50	501
Vent 3.0	387	1126	1.31	438
Vent 2.0	387	1093	1.05	351
Vent 1.0	387	992	0.66	221

There is a substantial drop in muzzle velocity due to just the movement of the piston. Note that the pistons used in the experiments have a diameter of 5.5 cm (chamber diameter), substantially larger than the gun tube diameter (3.5 cm). To quantify this effect, simulations are done with the piston diameter equal to the gun tube diameter. A reverse chambrage is put at the back of the chamber. The length of the chamber is adjusted so that the closed-breech case has the same muzzle velocity as before. The new piston is a scaled heavy piston. The mass is reduced proportional to the area change. Therefore, the mass drops from 35.9 to 14.5 kg. The gun mass is increased to keep the total mass the same. The shorter nozzle is used in the simulations.

Table 8 shows the results. Compared to table 7, the drop in muzzle velocity from piston motion is much less. For a given distance to vent opening, the smaller piston results in less of a drop in recoil momentum. For a direct comparison, consider a muzzle velocity of 1130 m/s. For the heavy piston, the vent distance is 4 cm and the recoil velocity is 1.50 m/s. For the smaller piston, the vent distance is 2 cm and the recoil velocity is 1.40 m/s. The smaller moving breech is more efficient.

Table 8. Heavy piston: no gun resistance, short nozzle, smaller piston, and comparison of simulations.

Configuration	Pressure (MPa)	Muzzle Velocity (m/s)	Recoil Velocity (m/s)	Momentum (N-s)
Closed breech	398	1175	3.15	1050
Nonventing	392	1158	3.09	1032
Vent 5.0	392	1157	1.97	657
Vent 4.0	392	1157	1.83	610
Vent 3.0	392	1155	1.65	550
Vent 2.0	392	1130	1.40	466
Vent 1.0	392	1049	1.01	335

If the nozzle is modified, the mass of the system will also be modified. However, this has almost no effect on the recoil momentum, which depends on the force exerted on the gun and the piston. Therefore, this was not considered in the previous calculations. Reducing the length of the nozzle would presumably reduce the system mass.

7. The 105-mm RAVEN Simulations

In this section, initial estimates of the behavior of the 105-mm demonstrator are made. The design uses standard JA2 stick propellant, so the combustion rate is known. There is no shear plug, and there are no crush tubes. Based on previous modeling of the cartridge, the projectile resistance is known. Unlike the 35-mm gun, everything required for the basic model is known.

In this report, the recoil brakes, recuperators, and forecoil pads are not included in the simulations. These designs are not yet finalized. The interest here is the efficiency of the basic concept.

There are six spindles that can be placed at the end of the piston (see figure 3). Unlike the 35-mm gun, the piston and the projectile have the same area. The end of the piston is just to the left of the normal breech location (x = 0.0). With spindle A, the vent opens after 5 cm of travel. The other pistons are cut away to open the vent sooner.

The inner part of the nozzle has a 25° angle out to –29.258 cm and then changes to a 20° angle out to –59.503 cm. The outer part of the nozzle (attached to the piston) has a 26° angle and originally goes to –108.8 cm. As the piston moves rearward, the nozzle will get longer.

Table 9 summarizes the results for the first spindle. In order to separate the effects, the gun is first modeled as a closed-breech system. The piston (with spindle A) is assumed to be fastened to the gun. The muzzle velocity of the projectile is noted. The system momentum (mass × velocity) after 50 ms is noted (units are kilogram-meters/second = newton seconds). Next, the gun is modeled as a nonventing system. The piston moves to the rear in a tube, but there is no nozzle or venting to the outside. The muzzle velocity drops slightly (less than 1%) due to the volume increase from the moving piston. The gun winds up with a small negative velocity (indicating rearward motion).

This gun has chambrage at both ends of the chamber. The negative velocity is primarily due to the pressure gradient. The pressure at the back of the chamber is slightly higher than the pressure at the front of the chamber. Most of the momentum is transferred to the piston. The system momentum is the vector sum of the gun and piston momentums. The system momentum is less than the closed-breech case due to the performance decrease.

Table 9. Spindle A: comparison of simulations.

Configuration	Muzzle Velocity (m/s)	Gun Momentum (N-s)	Piston Momentum (N-s)	System Momentum (N-s)
Closed breech	1470	—	—	–22441
Nonventing	1457	–257	–21416	–21673
Split nozzle	1457	2535	–13776	–11241
Inner nozzle	1457	2525	–13777	–11252
Short nozzle	1457	2158	–13770	–11612

Next, the code is run in the default configuration, with the split piston. The muzzle velocity is the same as with the nonventing piston. That is, venting occurs late enough that the rarefaction wave does not reach the projectile. The projectile does not know the difference between the venting and nonventing cases. The gun winds up with a relatively small forward motion, primarily from the inner part of the nozzle. The piston winds up with a larger rearward motion, due primarily to the breech pressure on the end of the spindle. The figure of merit is the sum of the momentums. This gives the force acting on the mount. The system momentum is reduced 50%; this is similar to the 35-mm gun with a smaller piston (section 6.5).

A larger nozzle is not necessarily helpful because the nozzle is overexpanded later in the firing cycle. The code is run with the outer part of the nozzle (attached to the piston) eliminated. The results are virtually identical to the default configuration. The increased thrust on the outer nozzle early in the firing cycle is matched by the increased drag late in the firing cycle, when the nozzle is overexpanded.

As a final check, the last section of the inner nozzle (20° angle) is eliminated. This cuts off more than half of the inner piston. The forward momentum of the gun is substantially reduced, but most of the momentum is in the piston. The system momentum is reduced 48% rather than the default of 50%. Therefore, a much smaller nozzle will work almost as well as the default split nozzle.

Table 10 summarizes the results for the second spindle. The vent opens after the piston moves 4.3 cm. The closed-breech velocity is slightly less because the initial system volume is slightly more. The nonventing case drops the muzzle velocity less than 1%. For the split nozzle, the muzzle velocity drops a little more. The rarefaction wave just reaches the projectile before muzzle exit. The reduction is recoil momentum is about 54%. Since the vent opens sooner, the nozzle is more efficient. The outer nozzle still has a negligible effect. The short nozzle again changes the system momentum only by about 2%.

Table 11 summarizes the results for spindle C. The vent opens after 3.7 cm. The vent has slightly more of an effect on the muzzle velocity. The recoil momentum drops another couple of percents. Again, the outer nozzle has only a very small effect.

Table 10. Spindle B: comparison of simulations.

Configuration	Muzzle Velocity (m/s)	Gun Momentum (N-s)	Piston Momentum (N-s)	System Momentum (N-s)
Closed breech	1466	—	—	–22387
Nonventing	1453	–253	–21387	–21640
Split nozzle	1451	2663	–13009	–10346
Inner nozzle	1451	2656	–13034	–10377
Short nozzle	1451	2264	–13027	–10763

Table 11. Spindle C: comparison of simulations.

Configuration	Muzzle Velocity (m/s)	Gun Momentum (N-s)	Piston Momentum (N-s)	System Momentum (N-s)
Closed breech	1465	—	—	–22428
Nonventing	1452	–252	–21382	–21635
Split nozzle	1445	2730	–12599	–9869
Inner nozzle	1445	2726	–12632	–9906
Short nozzle	1445	2323	–12657	–10303

Table 12 summarizes the results for spindle D. The vent opens after 2.6 cm. The venting now causes a substantial drop in muzzle velocity. The default split nozzle drops the recoil momentum by two thirds. As in previous analyses, the outer nozzle has only a small effect on the recoil, but going to the short nozzle has a substantial effect. Table 13 summarizes the results for spindle E. The vent opens after 1.9 cm. The changes are a little larger than spindle D.

Table 12. Spindle D: comparison of simulations.

Configuration	Muzzle Velocity (m/s)	Gun Momentum (N-s)	Piston Momentum (N-s)	System Momentum (N-s)
Closed breech	1455	—	—	–22334
Nonventing	1442	–241	–21308	–21549
Split nozzle	1394	3387	–10837	–7451
Inner nozzle	1394	3389	–10957	–7568
Short nozzle	1394	2899	–10956	–8057

Table 13. Spindle E: comparison of simulations.

Configuration	Muzzle Velocity (m/s)	Gun Momentum (N-s)	Piston Momentum (N-s)	System Momentum (N-s)
Closed breech	1452	—	—	–22326
Nonventing	1439	–238	–21291	–21530
Split nozzle	1345	3576	–9876	–6300
Inner nozzle	1345	3578	–10018	–6440
Short nozzle	1345	3063	–10020	–6958

Finally, table 14 summarizes the results for spindle F. The vent opens after 1.2 cm. There is a large drop in muzzle velocity (12%) from the closed-breech simulation. But the split nozzle default simulation drops the recoil momentum by 77%. The smaller nozzles make a noticeable difference in the final system momentum; but in terms of the drop from the closed-breech momentum, the difference is not substantial.

Table 14. Spindle F: comparison of simulations.

Configuration	Muzzle Velocity (m/s)	Gun Momentum (N-s)	Piston Momentum (N-s)	System Momentum (N-s)
Closed breech	1451	—	—	–22332
Nonventing	1438	–236	–21276	–21513
Split nozzle	1278	3776	–8861	–5085
Inner nozzle	1278	3776	–9016	–5241
Short nozzle	1278	3239	–9023	–5784

The recoil of the system can be reduced 50%, with a small drop in muzzle velocity, or more than 75%, with a large drop in muzzle velocity. The outer nozzle has very little effect on the recoil. Even the inner nozzle can be made smaller without a large recoil penalty. Of course, there may be other reasons for a large nozzle, such as blast reduction.

8. Conclusions

The 1-D RAVEN code has been updated. The same version of the code can now model the 35-mm RAVEN gun and the proposed 105-mm demonstrator.

There is a significant correction in the nozzle conditions. The 1-D code now more accurately models the nozzle when it is overexpanded. The pressure in the nozzle can be under atmospheric pressure for a significant amount of time. During this time, the nozzle produces negative thrust since the pressure on the outside of the nozzle is larger than the pressure inside the nozzle.

Due partially to this effect, the 35-mm nozzle and the proposed 105-mm nozzle are larger than necessary. The nozzles can be reduced significantly in size, with only a minor effect on the recoil. There may be other reasons for a large nozzle than recoil reduction, such as blast reduction.

For both basic gun designs, the code indicates that the recoil can be reduced 50%, with only a small decrease in the muzzle velocity. The recoil can be reduced by at least 75% if a large decrease in muzzle velocity is allowed.

9. References

1. Kathe, E. L. Rarefaction Wave Gun Propulsion. Ph.D. Thesis, Rensselaer Polytechnic Institute, Troy, NY, May 2002.

2. Coffee, T. P. *Modeling of the 35-mm Rarefaction Wave Gun*; ARL-TR-3792; U.S. Army Research Laboratory: Aberdeen Proving Ground, MD, May 2006.

3. Chinn, G. M. *The Machine Gun, Volume V*; Edwards Brothers Publishing: Ann Arbor, MI, 1987.

4. McNeil, J. Benet Laboratories, Watervliet, NY. Private communication, 2006.

5. Coffee, T. P. *A Combined Lumped Parameter/One-Dimensional Blowdown Model for the Regenerative Liquid Propellant Gun*; BRL-TR-3364; U.S. Army Ballistics Research Laboratory: Aberdeen Proving Ground, MD, June 1992.

6. Anderson, R. D.; Fickie. K. D. *IBHVG2 - A User's Guide*; BRL-TR-2829; U.S. Army Ballistics Research Laboratory: Aberdeen Proving Ground, MD, July 1987.

7. Gough, P. S. *Interior Ballistics Modeling: Extensions to the One-Dimensional XKTC Code and Analytical Studies of Pressure Gradient for Lumped Parameter Codes*; ARL-CR-460; U.S. Army Research Laboratory: Aberdeen Proving Ground, MD, February 2001.

8. Gough, P. S.; Zwarts, F. J. Modeling Heterogeneous Two-Phase Reacting Flow. *AIAA Journal* **1979**, *17* (1), 17–25.

9. Oerlikon. *Oerlikon 35 mm Ammunition*; publication WWW 400101 E 1978; Machine Tool Works Oerlikon-Buhrle Ltd.: Zurich, Switzerland, 1978.

NO. OF COPIES	ORGANIZATION
1 (PDF only)	DEFENSE TECHNICAL INFORMATION CTR DTIC OCA 8725 JOHN J KINGMAN RD STE 0944 FORT BELVOIR VA 22060-6218
1	DIRECTOR US ARMY RESEARCH LAB IMNE ALC HRR 2800 POWDER MILL RD ADELPHI MD 20783-1197
1	DIRECTOR US ARMY RESEARCH LAB RDRL CIM L 2800 POWDER MILL RD ADELPHI MD 20783-1197
1	DIRECTOR US ARMY RESEARCH LAB RDRL CIM P 2800 POWDER MILL RD ADELPHI MD 20783-1197
	ABERDEEN PROVING GROUND
1	DIR USARL RDRL CIM G (BLDG 4600)

NO. OF COPIES ORGANIZATION

2 DIRECTOR
US ARMY RESEARCH LAB
RDRL ROP
D MANN
R SHAW
TECH LIB
PO BOX 12211
RESEARCH TRIANGLE PARK NC
27709-2211

8 US ARMY AVN & MIS CMND
W CHEW
C DOLBEER
J LILLY
M LYON
J FISHER
B MARSH
R MICHAELS
D THOMPSON
REDSTONE ARSENAL AL
35898-5249

1 PM MAS
SFAE AMO MAS
M BUTLER
BLDG 354
PICATINNY ARSENAL NJ
07806-5000

9 DIR BENET WEAPONS LAB
M AUDINO
R BERGGREN
R DILLON
R FISCELLA
R HASENBEIN
E KATHE
J MCNEIL
K MINER
S SOPOK
WATERVLIET NY
12189-4050

1 COMMANDER
RADFORD ARMY AMMO PLANT
SMCAR QA HI LIB
RADFORD VA 24141-0298

1 COMMANDER
US ARMY ARDEC
AMSRD AAR EBM
R CARR
BLDG 65N
PICATINNY ARSENAL NJ
07806-5000

NO. OF COPIES ORGANIZATION

1 COMMANDER
US ARMY ARDEC
SFAE AMO CAS
R CIRINCIONE
BLDG 171M
PICATINNY ARSENAL NJ
07806-5000

1 COMMANDER
US ARMY TACOM ARDEC
AMSRD AAR AEE W
S EINSTEIN
BLDG 382
PICATINNY ARSENAL NJ
07806-5000

1 COMMANDER
US ARMY TACOM ARDEC
RDCOM
ATD AMSTA AR TDC
J HEDDERICH
BLDG 94
PICATINNY ARSENAL NJ
07806-5000

1 COMMANDER
US ARMY TACOM ARDEC
AMSRD AAR AEE W
P HUI
BLDG 382
PICATINNY ARSENAL NJ
07806-5000

1 COMMANDER
US ARMY ARDEC
AMSRD AAR D
J LANNON
BLDG 1
PICATINNY ARSENAL NJ
07806-5000

1 COMMANDER
US ARMY NGIC
AMXST MC 3
2055 BOULDERS RD
CHARLOTTESVILLE VA 22911-8318

1 COMMANDER
US ARMY ARDEC
AMSRD AAR AEM L
E LOGSDON
BLDG 65
PICATINNY ARSENAL NJ
07806-5000

NO. OF COPIES ORGANIZATION

1 COMMANDER
US ARMY ARDEC
AMSRD AAR ATD
B MACHAK
BLDG B1
PICATINNY ARSENAL NJ
07806-5000

1 COMMANDER
US ARMY TACOM ARDEC
AMSRD AAR AEE W
P O'REILLY
BLDG 407
PICATINNY ARSENAL NJ
07806-5000

1 COMMANDER
US ARMY TACOM ARDEC
AMSRD AAR AEE W
J O'REILLY
BLDG 382
PICATINNY ARSENAL NJ
07806-5000

1 COMMANDER
US ARMY ARDEC
SFAE AMO CAS
J RUTKOWSKI
BLDG 171M
PICATINNY ARSENAL NJ
07806-5000

1 COMMANDER
US ARMY TACOM ARDEC
AMSTA AR CCH A
A SEBASTO
BLDG 65S
PICATINNY ARSENAL NJ
07806-5000

2 COMMANDER
NAVAL RSRCH LAB
TECH LIB
J BORIS
WASHINGTON DC 20375-5000

1 COMMANDER
US ARMY TACOM ARDEC
AMSRD AAR AEE W
J SHIN
BLDG 382
PICATINNY ARSENAL NJ
07806-5000

NO. OF COPIES ORGANIZATION

1 COMMANDER
US ARMY ARDEC
AMSRD AAR AEE W
R SURAPANENI
BLDG 3022
PICATINNY ARSENAL NJ
07806-5000

1 COMMANDER
US ARMY ARDEC
AMSRD AAR AEE W
S NICOLICH
BLDG 65S
PICATINNY ARSENAL NJ
07806-5000

1 OFFICE OF NAVAL RSRCH
J GOLDWASSER
875 N RANDOLPH ST RM 653
ARLINGTON VA 22203-1927

1 NASA LANGLEY RSRCH CTR
D BUSHNELL
MS 110
HAMPTON VA 23681-2199

3 COMMANDER
NAVAL AIR WARFARE CTR
A ATWOOD
S BLASHILL
T PARR
CH1NA LAKE CA 93555-6001

1 AIR FORCE RSRCH LAB
MNME EN MAT BR
B WILSON
2306 PERIMETER RD
EGLIN AFB FL 32542-5910

1 AIR FORCE OFC OF SCI RSRCH
M BERMAN
875 N RANDOLPH ST
STE 235 RM 3112
ARLINGTON VA 22203-1768

1 DIR SANDIA NATL LAB
M BAER
DEPT 1512
PO BOX 5800
ALBUQUERQUE NM 87185

NO. OF COPIES	ORGANIZATION
2	DIR LAWRENCE LIVERMORE NL L FRIED M MURPHY PO BOX 808 LIVERMORE CA 94550-0622
1	CENTRAL INTELLIGENCE AGCY J BACKOFEN RM 4PO7 NHB WASHINGTON DC 20505
1	BATTELLE EAST SCI & TECH A ELLIS 1204 TECHNOLOGY DR ABERDEEN MD 21001-1228
2	JHU CHEM PROP INFO AGCY W HUFFERD R FRY 10630 LITTLE PATUXENT PKWY STE 202 COLUMBIA MD 21044-3200
1 (CD only)	OUSD (AT&L)/STRAT & TACT SYS MUNITIONS T MELITA 3090 DEFENSE PENTAGON RM 3B1060 WASHINGTON DC 20301-3090
1	BRIGHAM YOUNG UNIV DEPT OF CHEMICAL ENGRG M BECKSTEAD PROVO UT 84601
1	CALIF INST OF TECH F E C CULICK 204 KARMAN LAB MS 301 46 1201 E CALIFORNIA ST PASADENA CA 91109
1	ARROW TECH ASSOC INC 1233 SHELBURNE RD D 8 S BURLINGTON VT 05403
2	UNIV OF ILLINOIS DEPT OF MECH INDUSTRY ENGRNG H KRIER R BEDDINI 144 MEB 1206 N GREEN ST URBANA IL 61801-2978
5	PENN ST UNIV DEPT OF MECH ENGRG K KUO T LITZINGER G SETTLES S THYNELL V YANG UNIV PARK PA 16802-7501
1	ALLEGHENY BALLISTICS LAB PO BOX 210 ROCKET CENTER WV 26726
1	ALLIANT TECHSYSTEMS INC C CANDLAND MN07 LW54 5050 LINCOLN DR EDINA MN 55436
3	ATK AMMO & ENERGETICS RADFORD ARMY AMMO PLANT D WORRELL W WORRELL S RITCHIE RT 114 PO BOX 1 RADFORD VA 24141-0299
2	ATK THIOKOL P BRAITHWAITE R WARDLE PO BOX 707 BRIGHAM CITY UT 84302-0707
1	ATK ELKTON J HARTWELL PO BOX 241 ELKTON MD 21921-0241
1	BAE ARMAMENT SYS DIV J DYVIK 4800 E RIVER RD MINNEAPOLIS MN 55421-1498
1	GEN DYNAMICS ST MARKS H RAINES PO BOX 222 SAINT MARKS FL 32355-0222
1	GEN DYNAMICS ARM SYS J TALLEY 128 LAKESIDE AVE BURLINGTON VT 05401

NO. OF COPIES ORGANIZATION

1 HICKS AND ASSOC SAIC
I MAY
7990 SCIENCE APPLIC CT
VIENNA VA 22182

1 PAUL GOUGH ASSOC INC
P GOUGH
1048 SOUTH ST
PORTSMOUTH NH 03801-5423

2 VERITAY TECH INC
R SALIZONI
J BARNES
4845 MILLERSPORT HWY
E AMHERST NY 14501-0305

1 SRI INTRNTL
PROPULSION SCIENCES DIV
TECH LIB
333 RAVENWOOD AVE
MENLO PARK CA 94025-3493

ABERDEEN PROVING GROUND

1 CDR USAATC
RDRL HRM CH
STECS LI
R HENDRICKSEN
APG MD 21005

43 DIR USARL
RDRL WM
B FORCH
P PLOSTINS
RDRL WMB
M ZOLTOSKI
RDRL WMB A
T KOGLER
D LYON
RDRL WMB D
W ANDERSON
R BEYER
A BRANT
S BUNTE
T COFFEE (5 CPS)
J COLBURN
P CONROY
B HOMAN
A HORST
S HOWARD
P KASTE

NO. OF COPIES ORGANIZATION

A KOTLAR
C LEVERITT
R LIEB
K MCNESBY
M MCQUAID
A MIZIOLEK
J MORRIS
J NEWBERRY
M NUSCA
R PESCE-RODRIGUEZ
G REEVES
B RICE
R SAUSA
J SCHMIDT (2 CPS)
A WILLIAMS
E SCHMIDT
RDRL WMM
S MCKNIGHT
RDRL WMS
T ROSENBERGER
RDRL WMT
B BURNS
P BAKER
W CIEPIELA
RDRL WMT B
N ELDREDGE